

# Electronic Supplementary Information

## A new family of sunlight-driven bifunctional photocatalysts based on TiO<sub>2</sub> nanoribbon framework and bismuth oxohalide nanoplates

Xuebo Cao\*<sup>a</sup> Zhufeng Lu,<sup>a</sup> Lianwen Zhu,<sup>a</sup> Le Yang,<sup>a</sup> Li Gu,\*<sup>b</sup> Liling Cai,<sup>a</sup> and Jie Chen<sup>a</sup>

<sup>a</sup> School of Biology and Chemical Engineering, Jiaxing University, Jiaxing, Zhejiang 314001, China. E-mail: [xbcao@mail.zjxu.edu.cn](mailto:xbcao@mail.zjxu.edu.cn)

<sup>b</sup> School of Materials and Textile Engineering, Jiaxing University, Jiaxing, Zhejiang 314001, China.  
E-mail: [guli@mail.zjxu.edu.cn](mailto:guli@mail.zjxu.edu.cn)

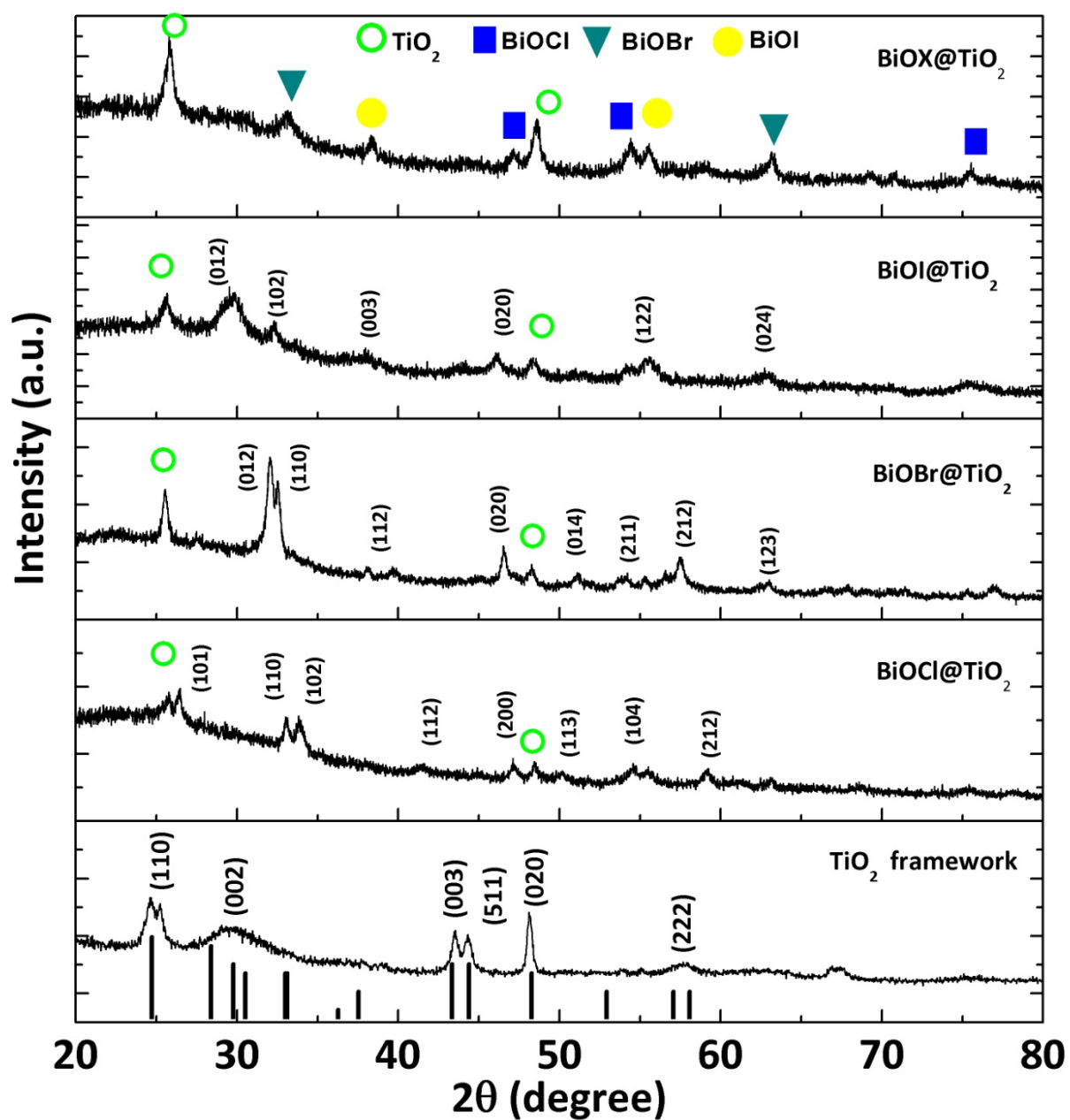


**Fig. S1.** XRD patterns of the pristine  $\text{TiO}_2$  framework and the hybrid frameworks. Standard XRD pattern of monoclinic  $\text{TiO}_2$  (i.e., vertical lines on the bottom of the figure) was also included for a comparison. The un-indexed peaks in the XRD pattern of  $\text{TiO}_2\text{-B}$  (around  $25.5^\circ$  and  $67^\circ$ ) was assigned to the (011) and (006) diffraction peaks of unconverted titanate.

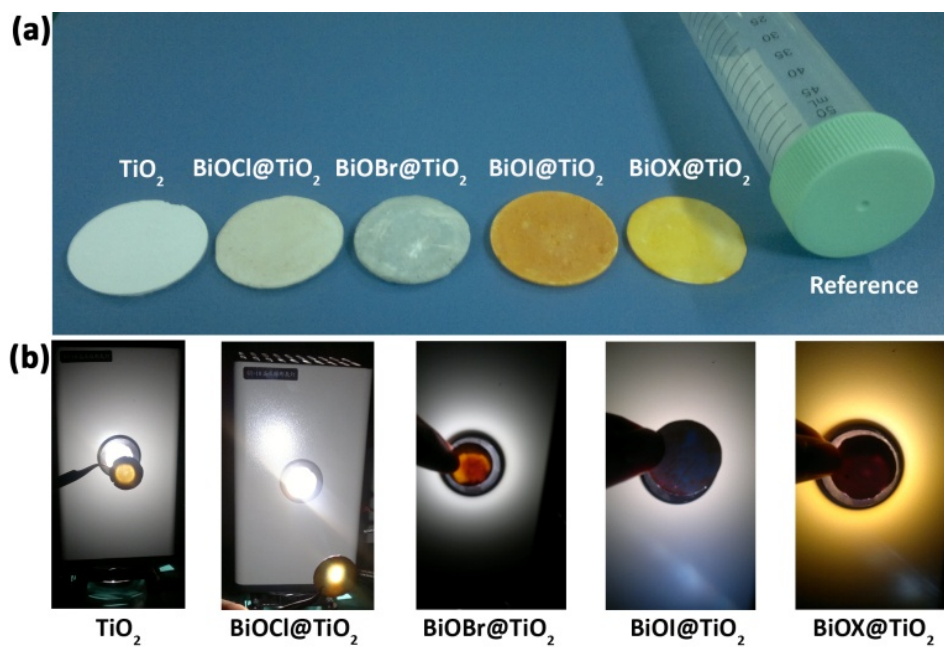


**Fig. S2** Photographs of the unmodified  $\text{TiO}_2$  nanoribbon framework and the hybrid  $\text{BiOCl@TiO}_2$ ,  $\text{BiOBr@TiO}_2$ ,  $\text{BiOX@TiO}_2$ , and  $\text{BiOI@TiO}_2$  frameworks. The 50 mL of centrifuge tube is included for scale. (b) Photographs of the frameworks illuminated by the beam from the Xeon lamp. They demonstrate that the frameworks are porous and penetrable to visible light.

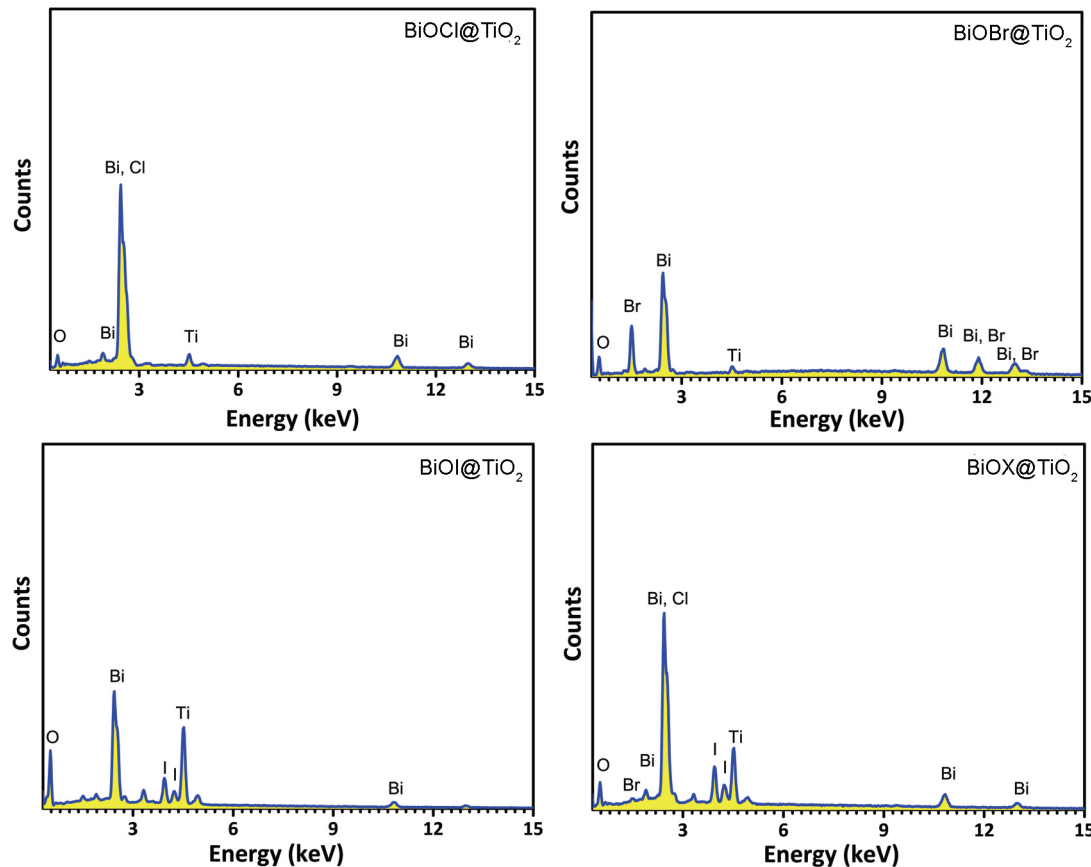


**Fig. S3** EDS spectra of various hybrid frameworks synthesized by using 0.05 M  $\text{Bi}(\text{NO}_3)_3$  and 0.05 M K. Quantitative EDS analysis indicates that the atomic ratio of Bi to X (X=Cl, Br, or/I) is

stoichiometric (around 1:1), while atomic ratios of Bi to Ti are 5.1:1 for  $\text{BiOCl}@\text{TiO}_2$ , 5.3:1 for  $\text{BiOBr}@\text{TiO}_2$ , 0.56:1 for  $\text{BiOI}@\text{TiO}_2$ , and 1.3:1 for  $\text{BiOX}@\text{TiO}_2$ .

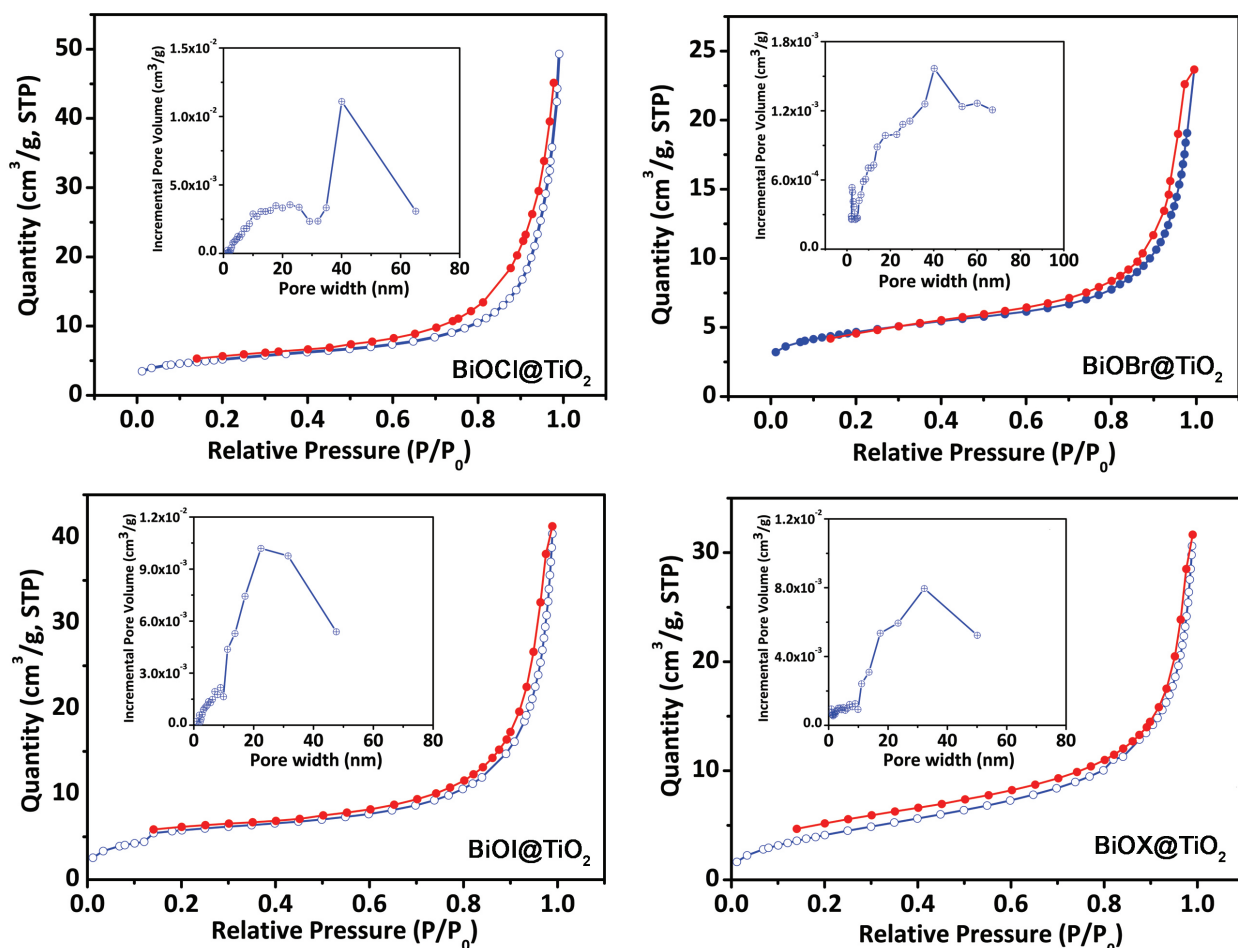


**Fig. S4** Nitrogen adsorption–desorption isotherms and the pore-size distribution plots (insets) of various hybrid frameworks at 77 K. The hysteresis loops suggest the presence of mesopores in the frameworks. The BET surface area were  $18.3 \text{ m}^2/\text{g}$  for  $\text{BiOCl}@\text{TiO}_2$ ,  $19.7 \text{ m}^2/\text{g}$  for  $\text{BiOBr}@\text{TiO}_2$ ,  $23.1 \text{ m}^2/\text{g}$  for  $\text{BiOI}@\text{TiO}_2$ , and  $16.0 \text{ m}^2/\text{g}$  for  $\text{BiOX}@\text{TiO}_2$ .

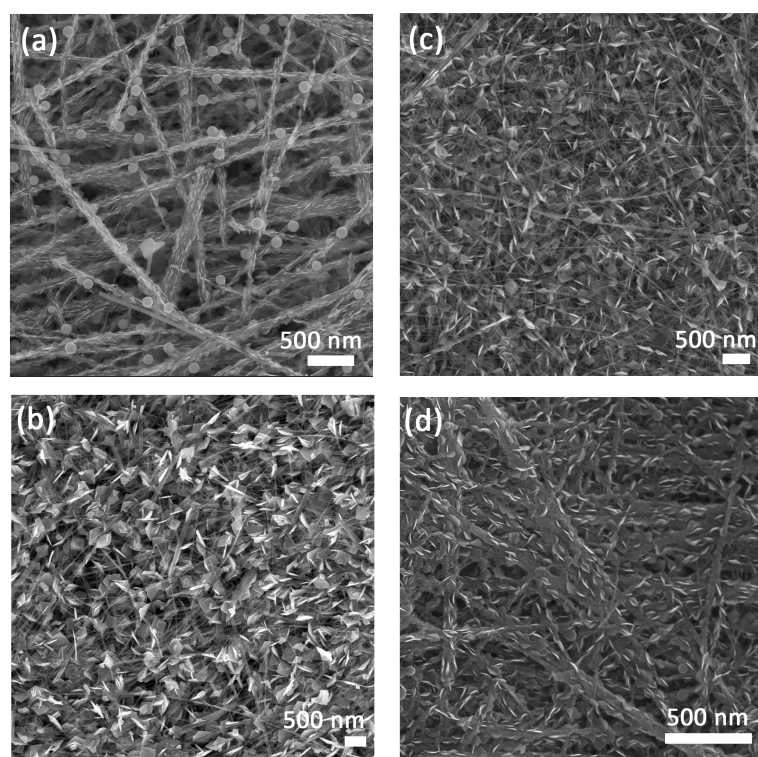


**Fig. S5** Panoramic SEM images of the surface of the hybrid frameworks synthesized by using 0.05 M  $\text{Bi}(\text{NO}_3)_3$  and 0.05 M KX. (a-d) corresponding to  $\text{BiOCl@TiO}_2$ ,  $\text{BiOBr@TiO}_2$ ,  $\text{BiOI@TiO}_2$ , and  $\text{BiOX@TiO}_2$ , respectively.

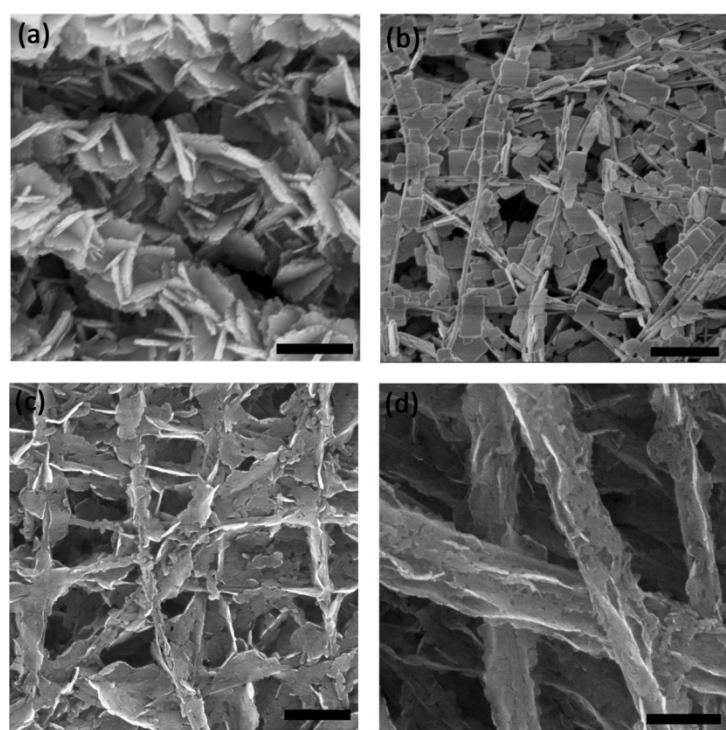


**Fig. S6** SEM images of the surface of the hybrid frameworks synthesized by using 0.075 M  $\text{Bi}(\text{NO}_3)_3$  and 0.075 M KX. (a-d) corresponding to  $\text{BiOCl@TiO}_2$ ,  $\text{BiOBr@TiO}_2$ ,  $\text{BiOI@TiO}_2$ , and

BiOX@TiO<sub>2</sub>, respectively. They reveal that the nanoribbons are encapsulated by dense nanoplates.

Scale bars: 500 nm.

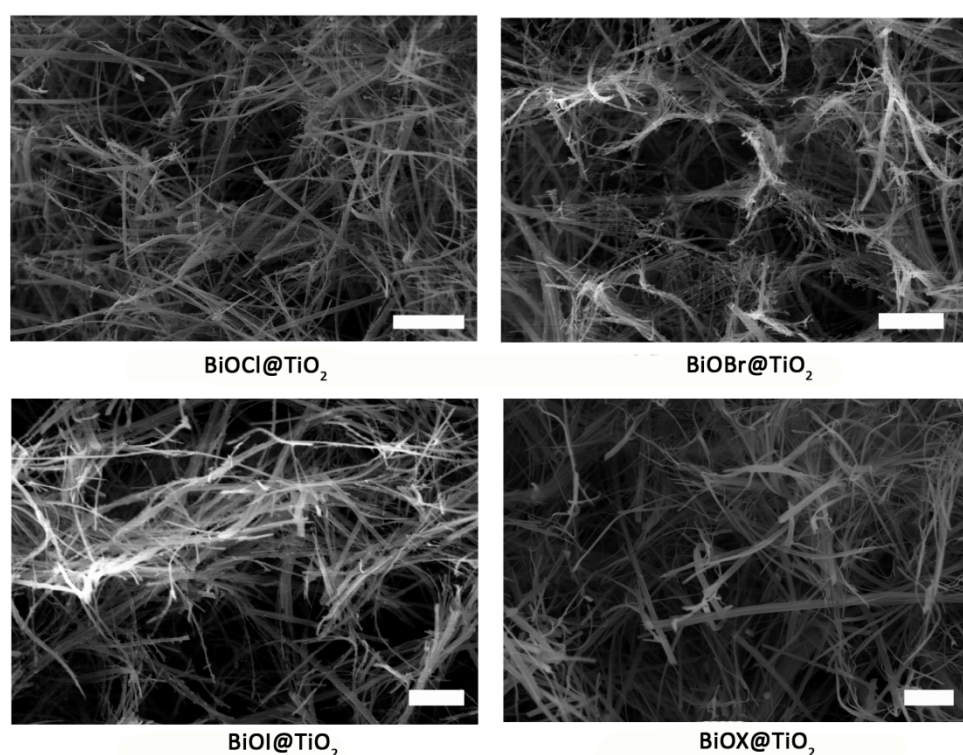


**Fig. S7** SEM images of the regions inside the hybrid frameworks, where the surface of the nanoribbon is free of nanoplates. Scale bars: 2  $\mu$ m.

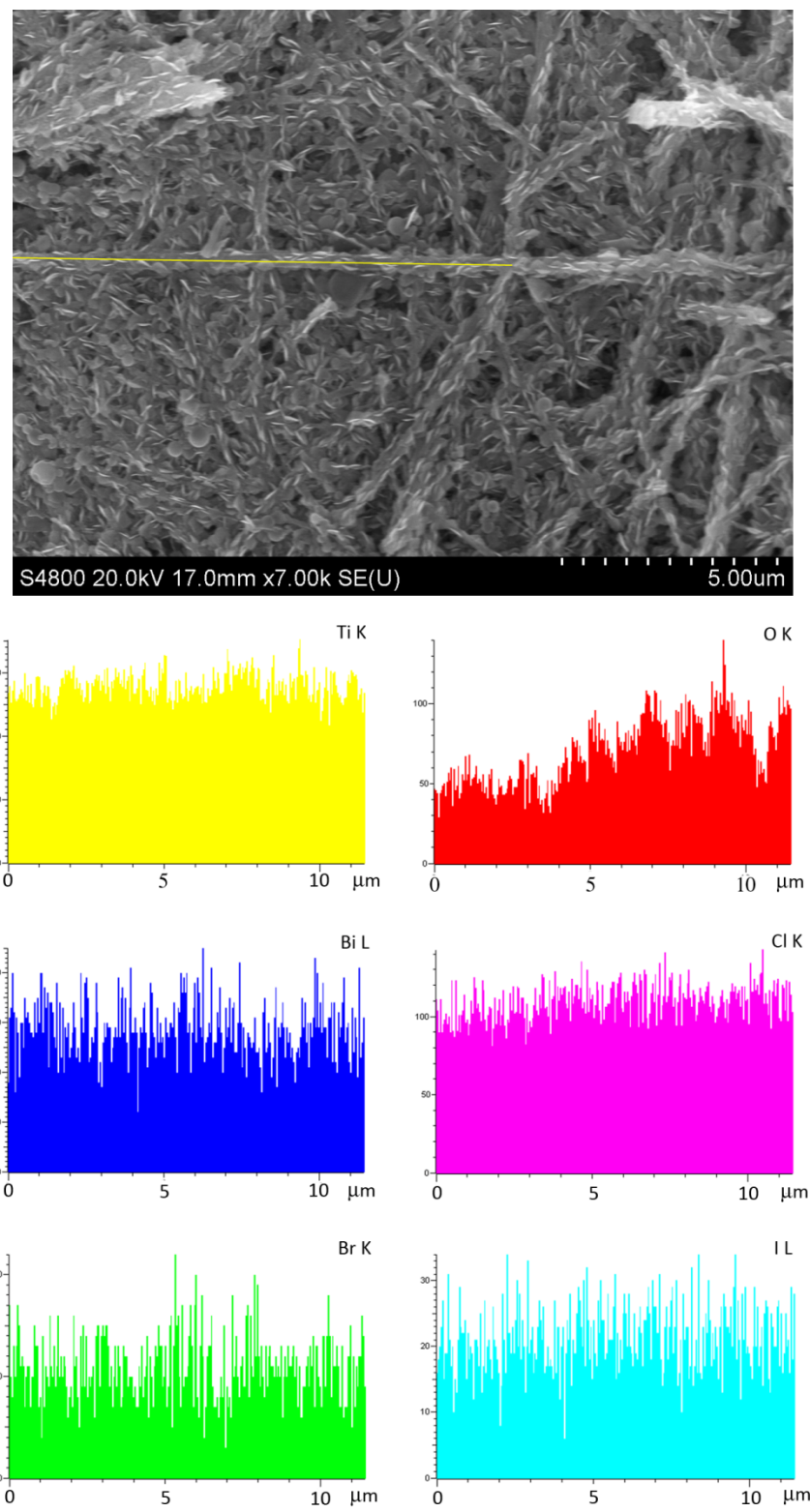


**Fig. S8** Element-sensitive mapping of the  $\text{BiOX}@\text{TiO}_2$  framework by the SEM-EDX system. The analysis was performed along the yellow line marked in the SEM image.

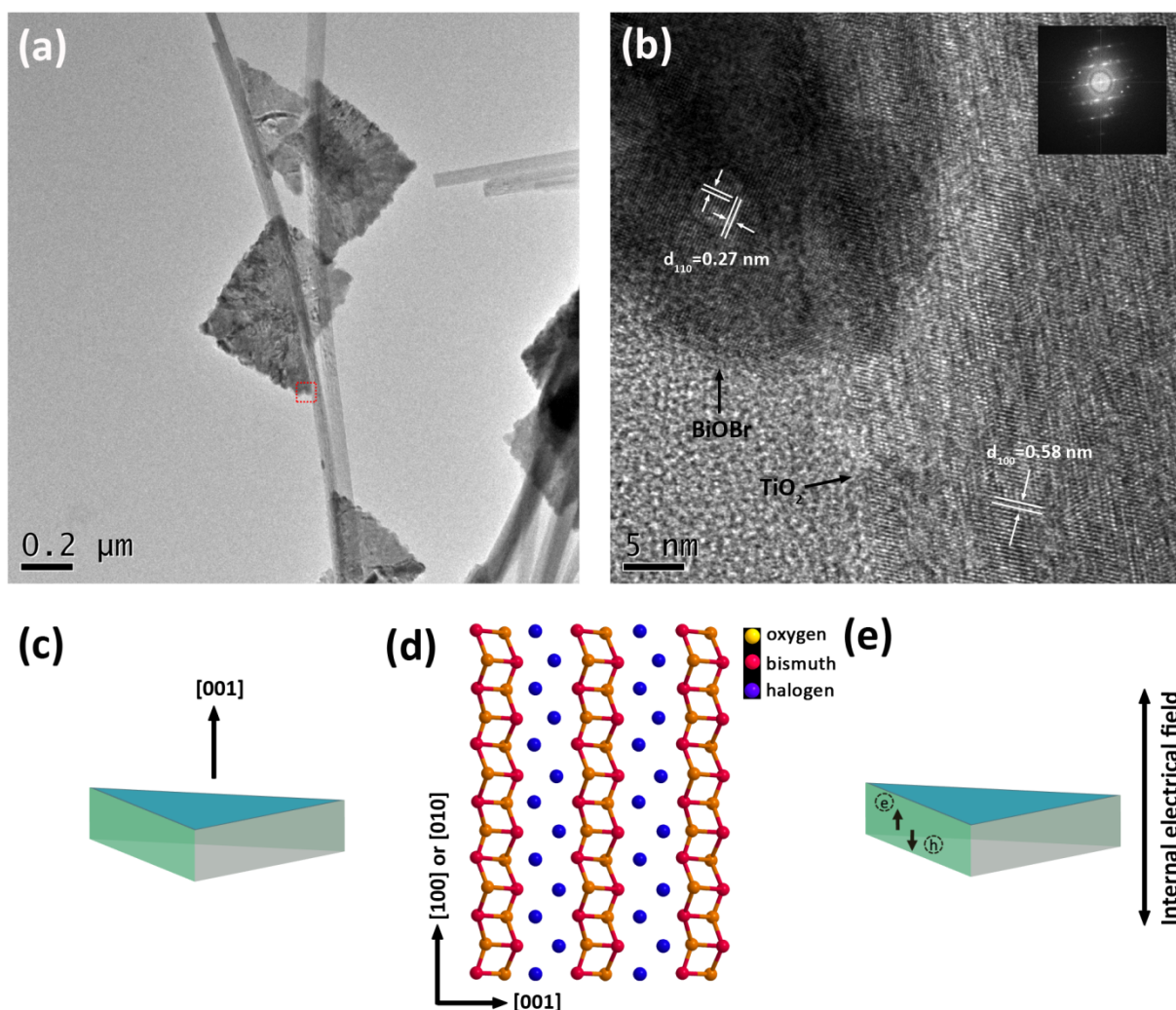


**Fig. S9** (a) TEM image of hybrid BiOBr@TiO<sub>2</sub> image. (b) HRTEM image showing the junction between BiOBr nanoplate and TiO<sub>2</sub> nanoribbon. The image was taken on the region marked by the square box shown in Part (a). (c) Schematic illustration of the crystal orientation of the nanoplate. (d) Schematic illustration of the crystal structure of bismuth oxohalides (blue spheres: halogen; orange spheres: oxygen; red spheres: bismuth). The alternative stacking of  $[\text{Bi}_2\text{O}_2]$  and halogen induces an internal static electrical field along the [001] direction. (e) Schematic illustration of the separation of photo-induced charges driven by the internal electrical field.

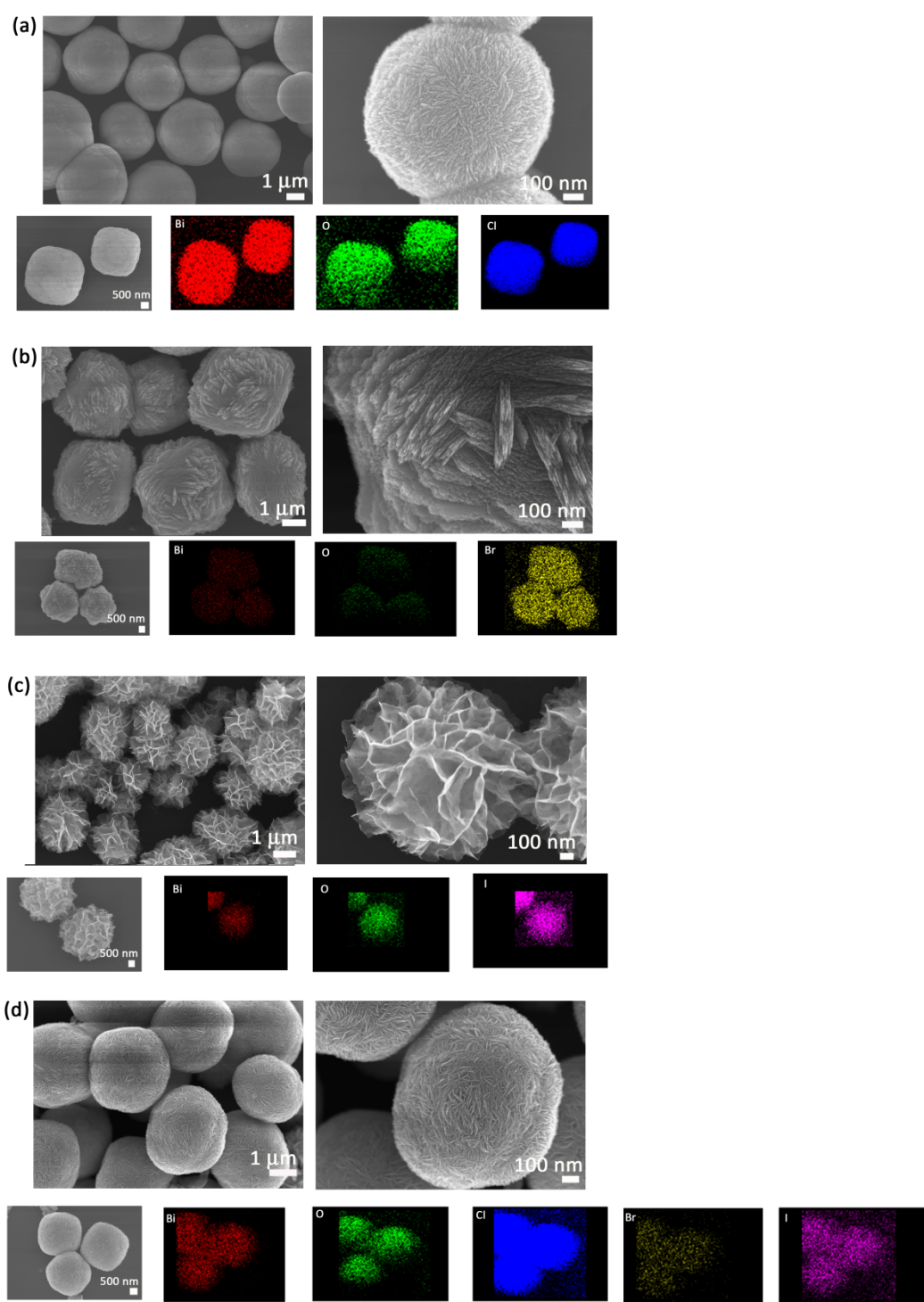


**Fig. S10** SEM images and EDS mapping of the free particles collected from the solution. These nanoparticles are found to be completely composed of bismuth oxohalides. (a-d) corresponding to the free particles collected from the systems for preparing  $\text{BiOCl@TiO}_2$ ,  $\text{BiOBr@TiO}_2$ ,  $\text{BiOI@TiO}_2$ , and  $\text{BiOX@TiO}_2$ , respectively. As seen, the free particles are not composed of discrete nanoplates, but instead of aggregated spherical superstructures.

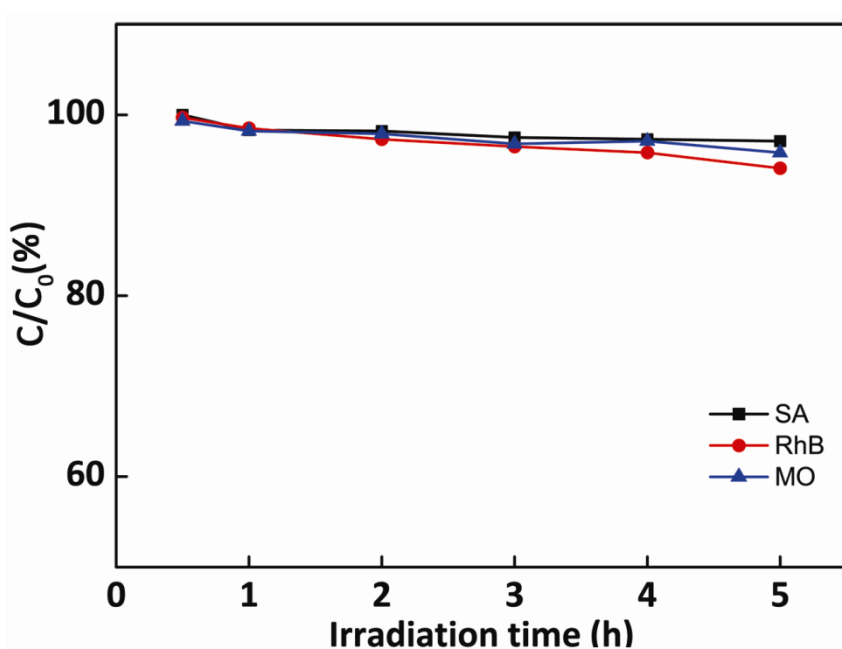


**Fig. S11** Concentration variation of the pollutants under the illumination of natural sunlight (without the photocatalyst).  $C_0$  and  $C$  indicate the initial concentration of the pollutants and the concentration of the pollutant at time  $t$ .

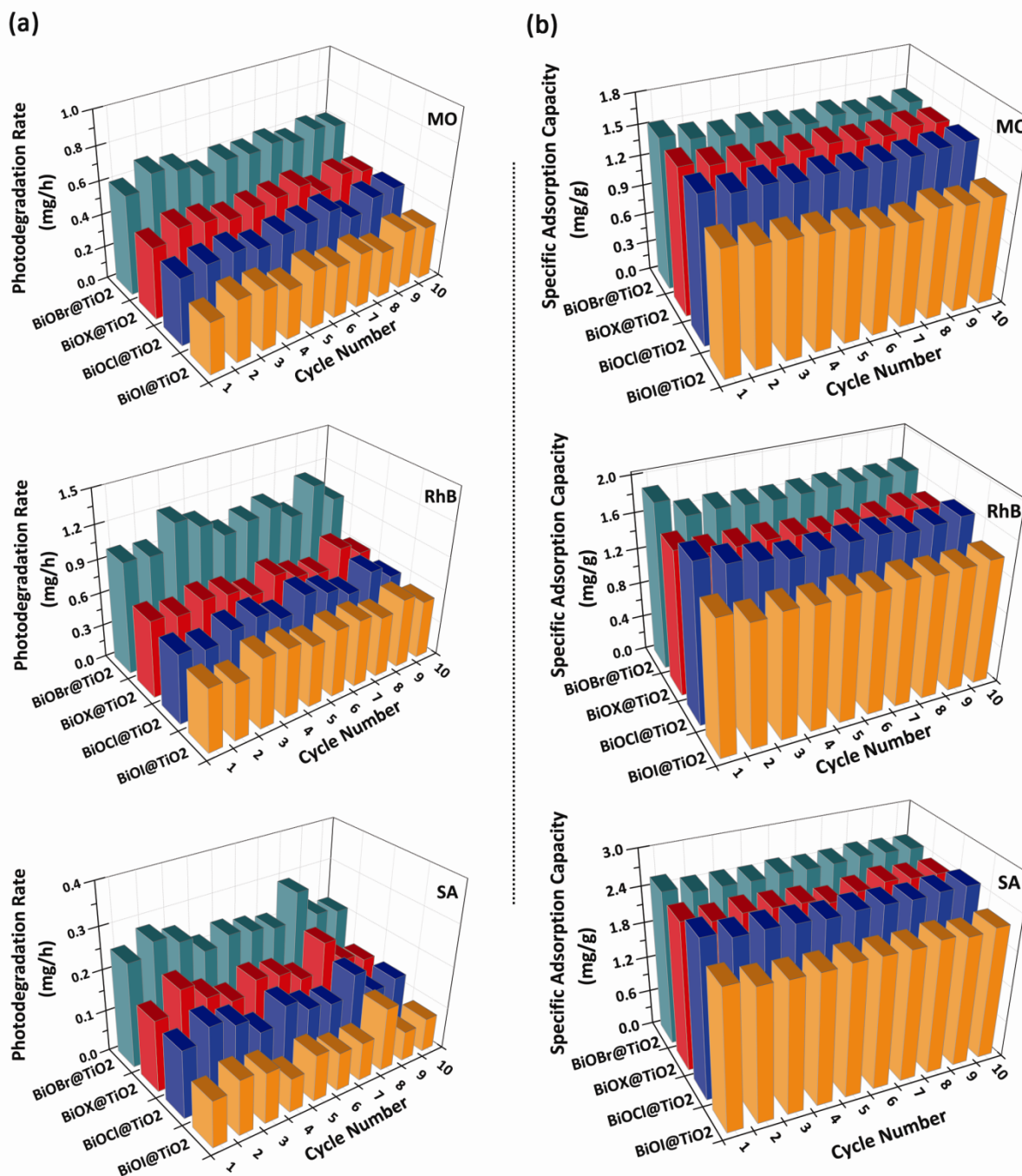


**Fig. S12** Cycling performances of the hybrid frameworks in the removal of pollutants. (a) Photodegradation rates of RhB, MO, and SA over the hybrid frameworks for 10 cycles, where the fluctuation is caused by the varied intensity of the sunlight. (b) Specific adsorption capacities of the hybrid frameworks for 10 cycles.